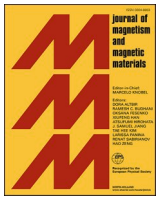
Journal of Magnetism and Magnetic Materials 629 (2025) 173350



Contents lists available at ScienceDirect

Journal of Magnetism and Magnetic Materials

journal homepage: www.elsevier.com/locate/jmmm



Research article



Comparison of micromagnetic modeling and experiment considering grain size distribution at 1–20 kHz

Wenbin Meng [a,b], Changgeng Zhang [a,b,*], Yongjian Li [a,b], Hao Zhang [a,b]

[a] State Key Laboratory of Intelligent Power Distribution Equipment and System, Hebei University of Technology, 300130 Tianjin, China
[b] Hebei Key Laboratory of Equipment and Technology Demonstration of Flexible DC Transmission, Hebei University of Technology, 300130 Tianjin, China

ARTICLE INFO

Keywords:
Nanocrystalline alloy
Magnetic properties test
Micromagnetic simulation
Grain size
Rotation of magnetic moment

ABSTRACT

The miniaturization and lightweight design of electrical equipment result in the widespread application of nanocrystalline alloys in high-frequency power electronic transformers and high-frequency switching power supplies. To elucidate the intrinsic correlation between mesoscopic magnetization behavior and macroscopic magnetic properties of nanocrystalline alloy, magnetic property measurement and micromagnetic modeling are performed on the 1K107B nanocrystalline alloy. The actual grain morphology characteristics are obtained through transmission electron microscopy (TEM) observation, and the three-dimensional micromagnetic simulation model with the same grain size statistical distribution is constructed. The broadband magnetic property test data are combined with mesoscopic theory to determine the key parameters for micromagnetic simulations. Comparative analysis between traditional model with the same grain size and the improved model constructed in this paper, it is found that in the prediction of loss density and coercivity, the average deviation between the improved model and the experimental data is less than 10%, showing higher prediction accuracy than the traditional model. These results indicate that micromagnetic model considering actual grain size distributions can more accurately reflect the magnetization mechanisms in nanocrystalline alloy.

1. Introduction

With the increasing demand for high power density and high-efficiency power converters, high-frequency magnetic components such as transformers and inductors often dominate the size of converters and lead to significant losses, making them a primary target for optimization. As a biphasic composite soft magnetic material, Nanocrystalline alloy features a microstructure in which nanoscale α-Fe(Si) grains are uniformly distributed within an amorphous matrix, with each grain randomly oriented [1]. Due to the unique microstructure of this alloy, it exhibits low anisotropy constant and magnetostrictive coefficient while also possessing excellent comprehensive magnetic properties such as high saturation magnetic induction, high initial permeability, low coercivity, and low core losses. These characteristics make it widely used in electromagnetic shielding, wireless charging, and high-frequency transformers [2–4].

The technical magnetization characteristics of nanocrystalline alloy can be explored from macroscopic and mesoscopic perspectives. At the macroscopic level, based on Ampère's circuital law and Faraday's law of induction, the magnetization characteristics of nanocrystalline alloy can be measured, including permeability, remanence, coercivity, and core loss [5,6]. Composition is the foundation for nanocrystalline alloy's functionality, while mesoscopic structure is the key to enhancing their performance. The differences in subsequent processing and applications of various materials depend on the differences in their mesoscopic structures [7].

At the mesoscopic scale, the dynamic behavior of magnetic domains in nanocrystalline alloy under external excitation can be observed using the magneto-optical Kerr effect. In the absence of applied stress, the random anisotropy in nanocrystalline alloy leads to irregular magnetic domain patterns. However, when stress is applied during the annealing process, the nanocrystalline alloy develops uniaxial anisotropy, forming stripe-like magnetic domains on the surface [8]. The surface magnetic domains of nanocrystalline alloy are observed using a high-speed camera. It is found that with the increase of the excitation frequency, the magnetic domains of nanocrystalline alloy with strong anisotropy strength change regularly, while the magnetic domains of nanocrystalline alloy with weak anisotropy strength change irregularly [9]. However, exploring the physical changes exhibited by nanocrystalline materials during the magnetization process and the underlying

* Corresponding author at:State Key Laboratory of Intelligent Power Distribution Equipment and System, Hebei University of Technology, 300130, Tianjin, China
E-mail address: changgeng.zhang@hebut.edu.cn (C. Zhang).

https://doi.org/10.1016/j.jmmm.2025.173350
Received 24 April 2025; Received in revised form 30 June 2025; Accepted 8 July 2025
Available online 11 July 2025
0304-8853/© 2025 Elsevier B.V. All rights are reserved, including those for text and data mining, AI training, and similar technologies.

mesoscopic mechanisms through experimental methods is still challenging [10].

To intuitively study the internal physical processes of magnetization in magnetic materials, micromagnetic simulations can be employed to visualize the magnetization process, compensating for the limitations of macro- and mesoscopic experiments [11,12]. The implementation of micromagnetic simulations involves linearizing the nonlinear Landau-Lifshitz-Gilbert (LLG) equation under the small-angle approximation to solve for the magnetization dynamics [13].

The random anisotropy model is investigated through numerical simulations, where the LLG equation is used to calculate the magnetization of grains with randomly oriented uniaxial anisotropic magnetic interactions. The simulation results yield the relationship between grain size and coercivity from the obtained magnetization curve [14]. A micromagnetic model is applied to simulate a nanocomposite $Nd_2Fe_{14}B$ permanent magnet with Fe_3B and α-Fe as soft magnetic phases. The simulation results indicated that grain size and phase distribution play significant roles in determining the magnetic properties of the magnetic material [15]. The effect of shape on the coercivity of nanosystems is also studied, demonstrating that shape anisotropy plays a critical role in coercivity by calculating the system's demagnetization factor [16].

A three-dimensional micromagnetic simulation model for nanocrystalline alloy is established using spherical unit cells as the basic structural unit, ensuring a consistent grain size. By varying the radii of the crystalline and amorphous phases, the volume fraction of the nanocrystalline alloy is adjusted. The study reveals that an increase in volume fraction results in higher losses [17]. Further, a three-dimensional mesoscopic model of nanocrystalline alloys is developed, taking a grain size of 10 nm as an example. In this model, spherical nanocrystals are uniformly distributed within an amorphous matrix. The effects of grain size, direct current bias, and nonsinusoidal excitation on the model are systematically analyzed [18,19]. The above micromagnetic simulation models utilize idealized microscopic structures and ideal micromagnetic parameters. However, the microscopic structure of magnetic materials plays a decisive role in their macroscopic magnetic properties, and structural differences can lead to variations in micromagnetic parameters. Therefore, it is necessary to conduct micromagnetic simulations that integrate the microscopic structure of magnetic materials with their macroscopic characteristics.

Regarding micromagnetic modeling of nanocrystalline alloy, this paper establishes a research framework integrating experimental characterization and numerical simulations. Based on the ring specimen method, the magnetic properties of the 1K107B nanocrystalline alloy are measured. Through theoretical derivation, the key parameters required for micromagnetic simulation are obtained, including the saturation magnetization M_s, the magnetic crystalline anisotropy constant K_1, and the exchange constant A. Utilizing grain size data obtained from TEM observation, an improved three-dimensional micromagnetic simulation model incorporating actual grain size distributions is developed. Comparative analysis between the improved model and traditional model with the same grain size demonstrates significantly enhanced consistency between simulated dynamic magnetic properties and experimental measurements in the proposed model. Additionally, the average magnetic moment rotational angular velocity is introduced to characterize the overall precession of the magnetic moment during the magnetization process, revealing the influence of excitation frequency on the average magnetic moment rotational angular velocity.

2. Establishment of micromagnetic simulation model for nanocrystalline alloy

2.1. Micromagnetic simulation model of nanocrystalline alloy

This study focuses on the 1K107B type nanocrystalline alloy with the chemical formula $Fe_{73.5}Cu_1Nb_3Si_{13.5}B_9$. It is formed by the annealing crystallization of an amorphous matrix, resulting in a two-phase structure composed of spherical nanocrystals and an amorphous matrix.

A small portion of the annealed nanocrystalline ribbon is observed under the bright field of TEM. As shown in Fig. 1, nanocrystals of varying sizes are randomly distributed within the amorphous matrix. Statistical analysis of the size and number of nanocrystals shows that the Gaussian distribution function of the grain size is

$$F(D) = \frac{1}{\sqrt{2\pi}\sigma} e^{-\frac{(D-14.26)^2}{2\sigma^2}} \tag{1}$$

where the standard deviation σ is 3.86 and D is the grain size. Eq. (1) can be abbreviated as $D \sim N(14.26, 14.9)$.

Based on the grain size distribution data obtained from TEM observations of the nanocrystalline alloy, a three-dimensional simulation model that reflects the actual grain size distribution is established, as shown in Fig. 2. Fig. 2(a) presents a schematic of the three-dimensional simulation model, which has dimensions of 480 nm × 240 nm × 20 nm, representing a localized region of the strip-like material that contains a single layer of multiple columns of nanocrystals of varying sizes. Fig. 2 (b) displays a two-dimensional cross-section of the nanocrystalline alloy in its initial state, where the blue circles of varying sizes represent the nanocrystals, the green substrate represents the amorphous material, and the randomly directed arrows indicate the magnetic moments. Since the sample is wound from the single nanocrystalline strip, it can be considered infinitely long in the longitudinal direction. In the experiment, the magnetic field strength is applied along its longitudinal direction. In the micromagnetic simulation, the excitation is applied in the length direction of 480 nm. Therefore, the periodic boundary condition is applied along the length direction to simulate the infinite length of the nanocrystalline magnetic ring.

2.2. Identification of simulation parameters

After being wound into a magnetic ring, the nanocrystalline ribbon undergoes the same annealing process, followed by measurements of its macroscopic magnetic properties.The high-frequency magnetic property testing system built using the ring sample method is shown in Fig. 3. The signal generator produces sine waveforms (1–20 kHz), amplified by the power amplifier to fully magnetize the sample. The current probe measures the primary winding current, the voltage probe captures the secondary winding's open-circuit voltage, and the digital oscilloscope records voltage and current signals in real time.

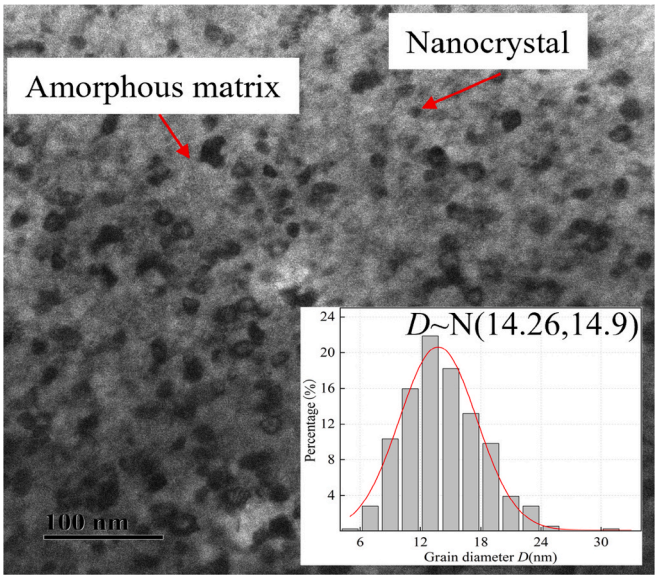
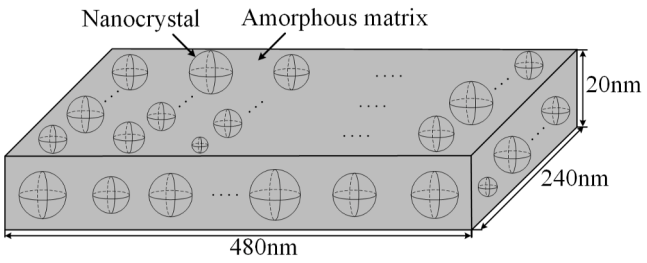
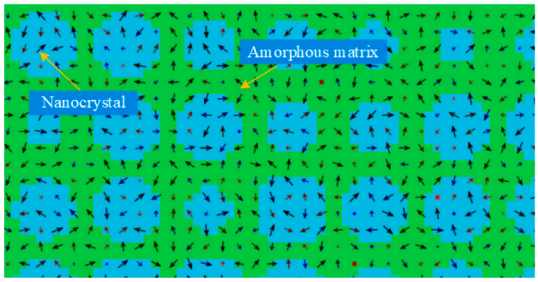


Fig. 1. Microstructure of nanocrystalline alloy.



(a) Schematic diagram of 3D simulation model



(b) Local cross-section of the simulation model

Fig. 2. Micromagnetic simulation model of nanocrystalline alloy.

2.2.1. Saturation magnetization

The magnetization curve of the nanocrystalline alloy measured in the experiment is shown in Fig. 4, with a saturation magnetization M_s of 9.4 $\times$ 10^5 A/m. The overall saturation magnetization of the nanocrystalline alloy is related to the saturation magnetization and volume fractions of each phase [20]. Multiple images obtained from TEM are analyzed using the open-source software Nano Measurer to individually measure the sizes of crystalline grains in each image. By distinguishing between crystalline and amorphous regions, the volume fraction of the crystalline phase in each image is calculated. The average crystalline volume fraction v_{cry} is determined by averaging the results from multiple images, yielding a value of 0.78. Consequently, the volume fraction of the amorphous phase v_{am} is calculated as 0.22. The saturation magnetization of the amorphous phase, M_{am}, is 9.23 $\times$ 10^5 A/m [21]. Therefore, the saturation magnetization of the crystalline phase, M_{cry}, can be obtained from Eq. (2).

2.2.2. Exchange interaction constant

The crystal phase is composed of $Fe_{80}Si_{20}$ with a exchange interaction constant A_{cr} of 10^{-11} J/m [22]. The exchange interaction constant of the amorphous matrix phase A_{am} can be obtained by

$$A_{am} = \frac{A_{ex} - A_{cr}v_{cr}}{v_{am}} \tag{3}$$

where A_{ex} is the average exchange interaction constant of 1.01 $\times$ 10^{-10} J/m [23].

The exchange interaction between the crystalline phase and the amorphous phase is given by

$$A_{cr-am} = \sqrt{A_{cr} \cdot A_{am}} \tag{4}$$

2.2.3. Magnetocrystalline anisotropy constant

The values of magnetic susceptibility χ are measured at different magnetic field strengths, and the relationship between χ and H^{-3} is shown in Fig. 5. Within a certain range of magnetic fields χ exhibits a linear relationship with H^{-3} with a proportionality constant of k. The coefficient b related to magnetocrystalline anisotropy can be obtained by Eq. (5) [24].

The randomly oriented nanocrystals are influenced by ferromagnetic exchange interactions, which reduce the effect of magnetocrystalline anisotropy, resulting in average anisotropy. The relationship between the average anisotropy constant $< K >$ and the coefficient b is as follows [25].

$$< K >= \frac{1}{2}\mu_0 M_s \sqrt{15b} \tag{6}$$

For nanocrystalline materials, ferromagnetic exchange interactions and the magnetocrystalline anisotropy field influence the atomic magnetic moments in each small grain simultaneously. Within the ferromagnetic exchange length L_{ex}, the magnetization direction is primarily governed by exchange interaction. Its realtion to the exchange interaction constant and the average anisotropy constant is [26]

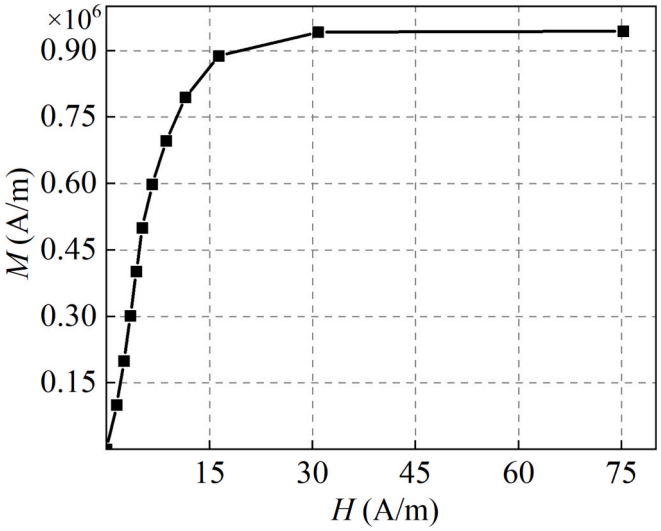


Fig. 4. Magnetization curve of nanocrystalline alloy.

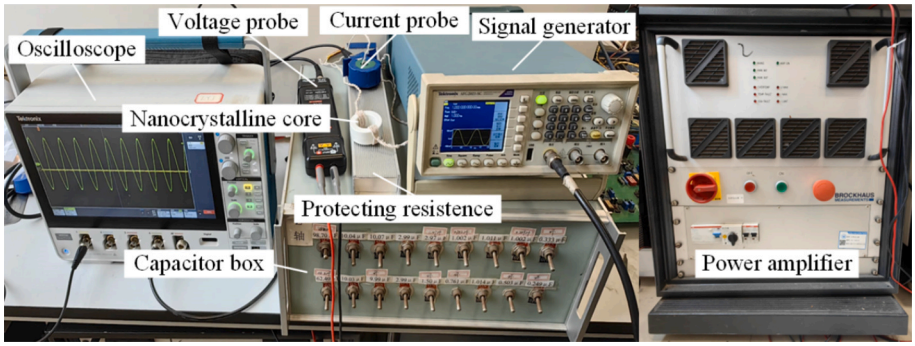


Fig. 3. High frequency magnetic properties testing system.

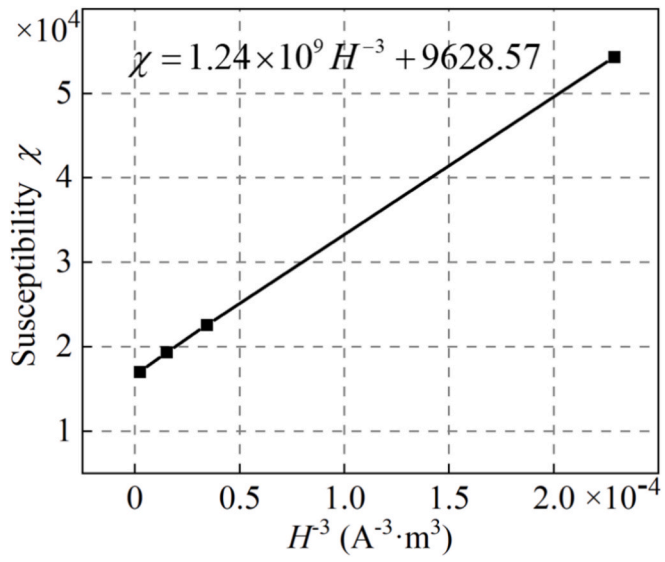


Fig. 5. Relationship between χ and H^{-3} of nanocrystalline alloy.

$$L_{ex} = \frac{1}{(1-\nu_{am})^{1/3}} \frac{D}{\frac{D}{\sqrt{A_{cr}/<K>}} + \frac{\Lambda}{\sqrt{A_{am}/<K>}}} \tag{7}$$

with

$$\Lambda = D\left[(1-\nu_{am})^{-1/3} - 1\right] \tag{8}$$

The relationship between the average anisotropy and the matnetocrystalline anisotropy is

$$K_1 = \frac{<K>}{\sqrt{1-\nu_{am}}} \left(\frac{L_{ex}}{D}\right)^{\frac{3}{2}} \tag{9}$$

Ultimately, the various parameters required for the micromagnetic simulation model of the nanocrystalline alloy can be obtained through Eqs. (3) to (9), as shown in Table 1.

2.3. The energy term of micromagnetic simulation

Due to the fact that the saturation magnetostriction coefficient λ_s of nanocrystalline alloy after annealing is only 2×10^{-6} m/m, the influence of magnetoelastic effects is neglected in the micromagnetic simulation. The total Gibbs free energy of magnetic materials includes exchange energy E_{exch}, Zeeman energy E_{ext}, magnetocrystalline anisotropy energy E_{ani}, and the demagnetization energy E_{dem} [27].

$$E_{total} = E_{exch} + E_{ext} + E_{ani} + E_{dem} \tag{10}$$

According to Brown's theory, the effective field $\boldsymbol{H}_{eff}$ is the derivative of the energy density with respect to the unit magnetization vector $\boldsymbol{m}$

$$\boldsymbol{H}_{eff} = -\frac{1}{\mu_0 M_s V} \frac{\partial E_{total}}{\partial \boldsymbol{m}} \tag{11}$$

where V is the volum of simulation model.

In this study, only alternating current excitations are applied to the micromagnetic simulation model, and thus the LLG equation solver is employed.

$$\frac{\mathbf{d}\boldsymbol{m}}{\mathbf{d}t} = -\gamma_0 (m \times \boldsymbol{H}_{eff}) + \alpha \left[\boldsymbol{m} \times \frac{\mathbf{d}\boldsymbol{m}}{\mathbf{d}t}\right] \tag{12}$$

Where γ_0 is the gyromagnetic ratio, α is the damping coefficient.

2.4. Excitation waveform

Due to the nonlinear magnetic properties of the nanocrystalline alloy, the current waveform on the primary side will become distorted as the magnetic flux density increases, resulting in a distortion of H. Therefore, to ensure the accuracy of the simulation, it is essential to consider the distortion factors of the excitation waveform in the simulation.

The actual excitation waveform in the experiment can be fitted using the Fourier series of Eq. (13), allowing for the determination of the actual H waveform at different excitation frequencies. The validity of the fitted waveform is determined by the root mean square error (RMSE) calculated from Eq. (14). Given the slight asymmetry of the actual waveform, the validity of the waveform is judged by whether the root mean square error is less than 1 A/m.

$$\widehat{H}(t) = a_0 + \sum_{n=1}^{N} [a_n \cos(n w_0 t) + b_n \sin(n w_0 t)] \tag{13}$$

Where a_0 is a constant, w_0 is the natural frequency, and a_n and b_n are the fitting coefficients.

$$\mathbf{RMSE} = \sqrt{\frac{\sum_N (\widehat{H}_i - H_i)^2}{N}} \tag{14}$$

Where $\widehat{H}_i$ is the fitted data, and H_i is the experimental data.

Fig. 6 presents the fitting results of the excitation waveform at an excitation frequency of 10 kHz. As shown in Fig. 6(a), with the increase in the order of the Fourier series, the fitted waveform increasingly approaches the experimental waveform. Fig. 6(b) visually illustrates the variation of the RMSE concerning the order, along with the pointwise residuals of the excitation waveform when N is at the highest order.

Table 2 presents the fitting results of the H waveform at various frequencies, with all fitting waveforms exhibiting RMSE and average residuals both less than 1. It is evident that with the increase in excitation frequency, the degree of waveform distortion intensifies, requiring a higher order for the fitting process.

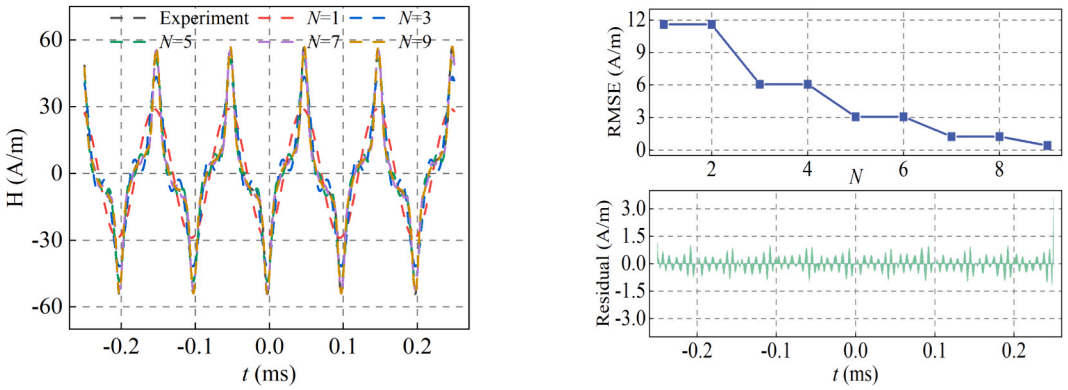
3. Validation of the simulation model

The micromagnetic parameters derived in Section 2.2 are incorporated into the simulation model, and an actual excitation waveform is applied to the improved model. As illustrated in Fig. 7, when a 10 kHz sinusoidal excitation is applied in the x-direction during the simulation, if the material reaches saturation, the output normalized magnetization in the x-direction, M_x, will be ± 1, while M_y and M_z will exhibit fluctuations around zero. Significant variations in the normalized magnetization in the other two directions occur only when the unit magnetic moment vector $\boldsymbol{m}$ flips. This is because,in a state of positive or negative saturation, the effective field $\boldsymbol{H}_{eff}$ is aligned parallel to the direction of the applied field. Switching between these two saturation states also causes the effective field $\boldsymbol{H}_{eff}$ to flip, increasing the components along the y-axis and z-axis as the unit magnetic moment vector $\boldsymbol{m}$ flips with the effective field $\boldsymbol{H}_{eff}$.

The middle section of the simulation model along the length direction is selected. Since the magnetization is carried out along the x-direction in the simulation, only the changes of the magnetic moment components in the xy plane are observed. The angle radian of each

Table 1
Simulation parameters of nanocrystalline alloy.

Micromagnetic parameter	Crystalline phase	Amorphous phase
M_s (A/m)	9.45×10^5	9.23×10^5
K_1 (J/m^3)	1.12×10^4	0
A (J/m)	1×10^{-11}	4.24×10^{-10}
L_{ex} (nm)	83.3	
$<K>$ (J/m^3)	584.7	



(a) Magnetic field strength waveform fitting (b) Fourier series fitting error

Fig. 6. Comparison between the fitted waveform and the experimental waveform.

Table 2
Fitting results of the excitation waveform.

Frequency	*N*	RMSE (A/m)	Average residual (A/m)
1 kHz	8	0.65	0.91
5 kHz	9	0.49	0.40
8 kHz	9	0.50	0.41
10 kHz	9	0.42	0.34
16 kHz	13	0.81	0.75
20 kHz	15	0.67	0.53

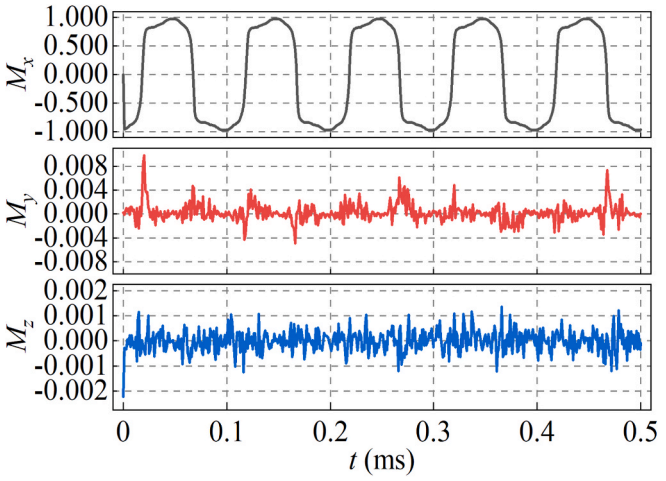


Fig. 7. The components of the normalized magnetization vector ***M*** in each direction.

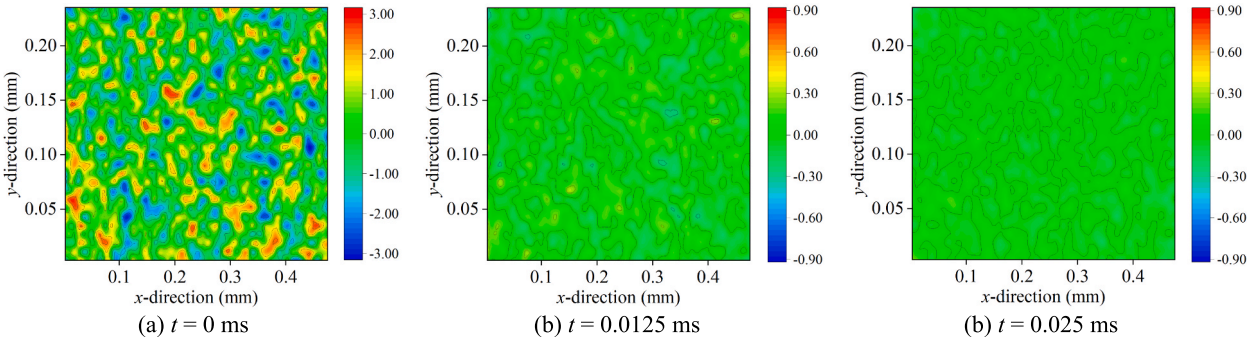
magnetic moment about the x-axis can be calculated by Eq. (15). Fig. 8 shows the magnetic moment distribution of the cross section of the simulation model within a quarter cycle under 10 kHz excitation. In the static magnetic state, the directions of the magnetic moments are different to ensure the minimum energy of the system. The overall magnetic moment gradually aligns with the x-axis as the magnetic field strength increases. When saturation is reached, the angle between all magnetic moments and the *x*-axis is 0 rad.

An alternating excitation in the frequency range of 1–20 kHz is applied to the established micromagnetic model, resulting in the dynamic magnetic hysteresis loop of the simulation model. Fig. 9 compares the simulated and experimentally measured hysteresis loops for different frequencies of alternating excitation. The simulation results exhibit a reasonable degree of overlap with the experimental results.

The area enclosed by the dynamic magnetic hysteresis loops in Fig. 9 is integrated, and the loss density of the nanocrystalline alloy is obtained from both experimental measurements and simulations under different frequency excitations. Table 3 presents the loss density obtained from experiments and simulations at different excitation frequencies and the errors between the two.

4. Analysis of the simulation results

In the micromagnetic simulations of nanocrystalline alloy, the ideal simulation model employs uniform grain sizes, which deviates from actual observations and affects the distribution of key micromagnetic parameters within the simulation model. This section compares the simulation results of the improved model with those of the ideal model, validating the accuracy of the improved model while also revealing the impact of grain size variation on macroscopic magnetic properties.



(a) $t = 0$ ms (b) $t = 0.0125$ ms (b) $t = 0.025$ ms

Fig. 8. The distribution of magnetic moments at different time intervals.

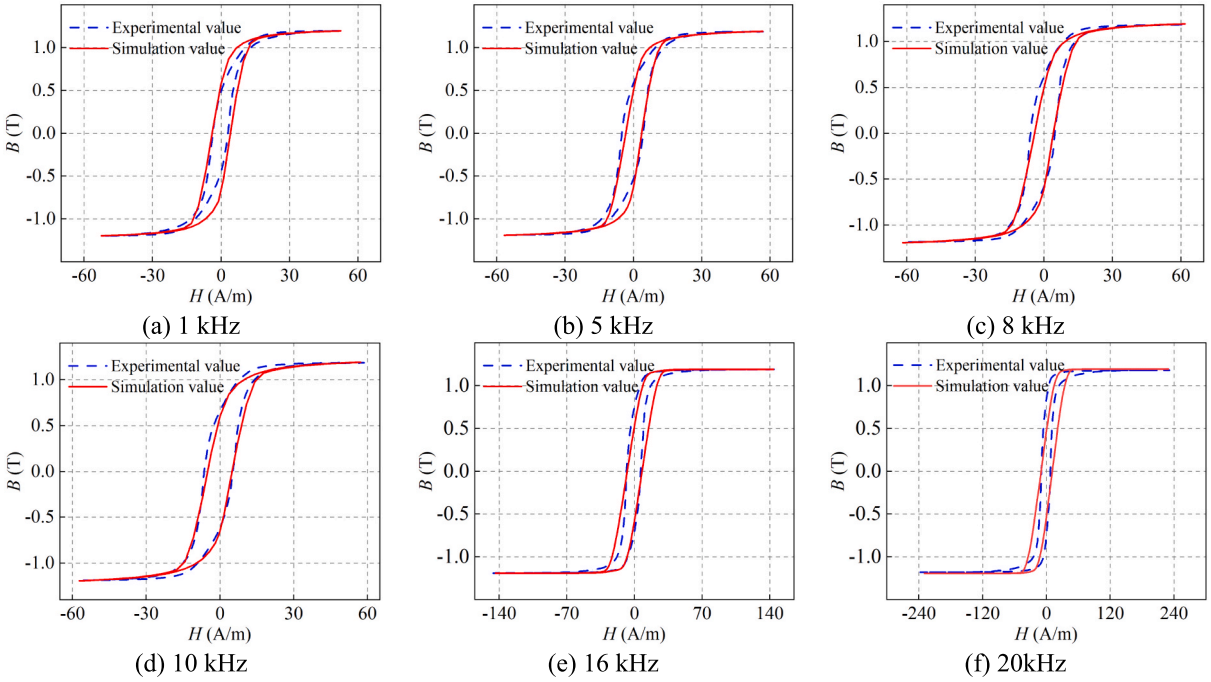


Fig. 9. Comparison of simulation and experiment under various frequency excitation.

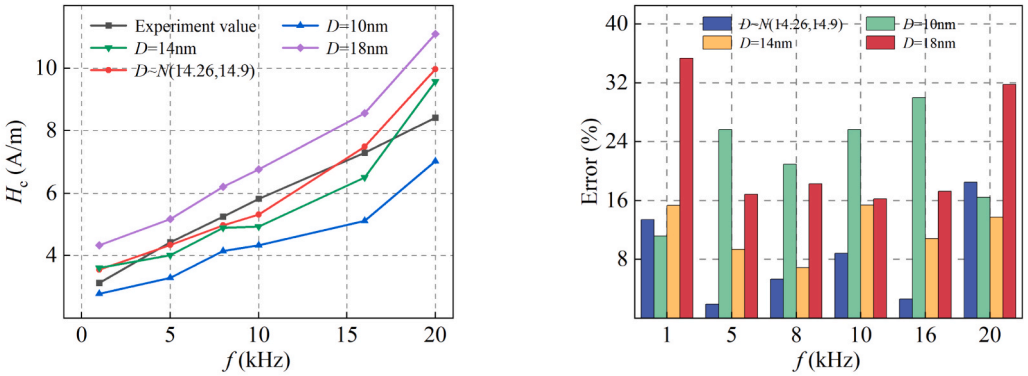
Table 3
Comparison of experimental data and simulation data on loss density of nanocrystalline alloy.

Frequency	Experimental value (W/kg)	Simulation value (W/kg)	Error(%)
1 kHz	1.58	1.69	6.69
5 kHz	13.08	12.75	2.52
8 kHz	20.97	19.47	7.17
10 kHz	29.46	27.82	5.56
16 kHz	70.3	62.89	10.54
20 kHz	119.95	105.64	11.93

4.1. Coercivity and loss density

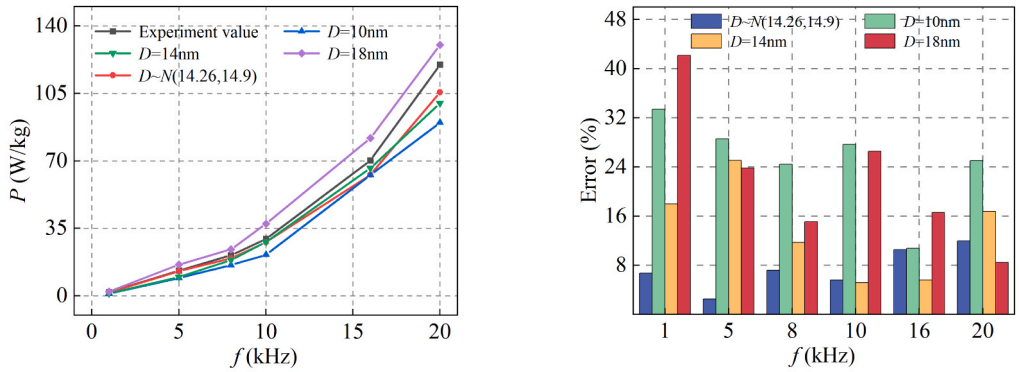
Fig. 10 presents the comparison of coercivities obtained from different simulation models with experimental values. As shown in Fig. 10(a), the coercivity gradually increases with the increase in frequency and grain size. The simulation results are closer to the experimental values when the grain size follows the Gaussian distribution. According to the Herzer model, the coercivity-grain size relationship follows $H_c \propto D^6$. Theoretical calculations predict 34-fold increase in coercivity when the grain size increases from 10 nm to 18 nm. For two-dimensional grain packing, this scaling reduces to approximately $H_c \propto D^2$, which is expected to produce 3.24-fold increase. However, as evidenced in Fig. 10(a), the increase obtained by simulation is significantly smaller. This deviation arises from the grain size distribution reduce the effective dimensionality of grain packing, which lead to a weaker increase in coercivity with grain size [28]. The errors of different simulation models are illustrated in Fig. 10(b), where the overall error for simulation models with grain sizes of 10 nm and 18 nm is significantly higher than that of the other two models. When the grain size follows the Gaussian distribution, the average error of the coercivity reach its minimum of 8.43 %.

From Fig. 11(a), it can be observed that the loss density gradually increases with the increase in frequency and grain size. When the grain sizes are 18 nm and 10 nm, the simulation results deviate significantly from the experimental values. The simulation results are much closer to the experimental values when the grain size follows the Gaussian distribution. The coercivity and the loss density are positively related, which indicates that the reduced effective dimensionality suppressing the growth of coercivity similarly governs the increase of loss density. From the error comparison in Fig. 11(b), it can be observed that when



(a) Comparison of coercivities for different grain sizes (b) Coercivity errors for different grain sizes

Fig. 10. Coercivity analysis of each simulation model.



(a) Comparison of loss densities for different grain sizes (b) Loss density errors for different grain sizes

Fig. 11. Loss density analysis of each simulation model.

the grain size follows the Gaussian distribution, the error in the simulated loss density is minimized, further demonstrating the effectiveness and accuracy of the improved model.

4.2. Angular velocity of magnetic moment rotation

In the simulation, the vector information of all unit magnetic moment vectors is recorded at various time points. The deflection angle of each unit magnetic moment vector relative to the direction of the applied field at different moments can be calculated using Eq. (16). By dividing the difference in deflection angles at adjacent time points by the corresponding time interval, the angular velocity of unit magnetic moment vector over that period can be obtained. Taking the average of the angular velocities of all unit magnetic moment vectors during the time interval yields the average rotational angular velocity of the magnetic moment vector.

$$\overline{\omega} = \frac{1}{nk}\sum_{i=1}^{n}\sum_{j=1}^{k}\left|\frac{\varphi_{ij}-\varphi_{i(j-1)}}{t_{ij}-t_{i(j-1)}}\right| \tag{16}$$

The variation of average rotation angular velocity of simulation models with different grain sizes is shown in Fig. 12. As the frequency increases, the average rotational angular velocity gradually increases. As the frequency increases, the average rotational angular velocity gradually rises. Combined with Fig. 11, it can be obtained that as the grain size increases, the coercivity of the material gradually increases, and its average magnetic moment rotation angular velocity slows down; that is, the material is difficult to magnetize; on the contrary, the average magnetic moment rotation angular velocity becomes faster, making the material easy to magnetize. When the grain size of the simulation model is 10 nm, the coercivity is at its minimum, and the average rotational angular velocity of the magnetic moment is at its maximum.

5. Conclusion

In this study, a three-dimensional micromagnetic simulation model incorporating grain size following Gaussian distribution is developed based on TEM observation. A systematic approach integrating mesoscopic theory with macroscopic experiments is employed to extract key micromagnetic parameters for both crystalline and amorphous phases in the simulations. The nonlinear saturation characteristics are rigorously considered through Fourier series decomposition to accurately reconstruct experimental excitation waveform. The results indicate that the reduction in the effective dimensionality of grain packing mitigates the rate at which coercivity and loss density increase with grain size. Compared to models with uniformly sized grains, when the grain size follows the Gaussian distribution, the average error in coercivity and loss density is less than 10 %. Furthermore, simulation results indicate

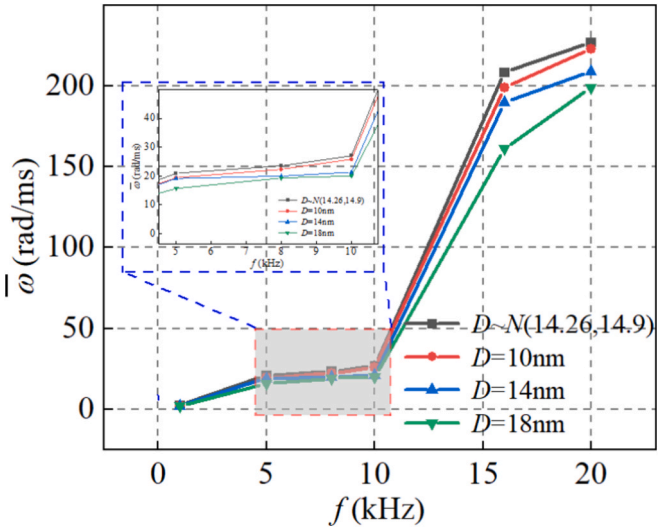


Fig. 12. Average magnetic moment rotation angular velocity.

that increasing grain size correlates with rising loss density and coercivity, accompanied by a deceleration in average rotational angular velocity of the magnetic moment vector, thereby exacerbating magnetization difficulty in nanocrystalline alloys.

CRediT authorship contribution statement

Wenbin Meng: Writing – original draft, Methodology, Data curation. **Changgeng Zhang:** Writing – review & editing, Supervision, Funding acquisition. **Yongjian Li:** Writing – review & editing, Funding acquisition. **Hao Zhang:** Validation, Software.

Declaration of competing interest

The authors declare that they have no known competing financial interests or personal relationships that could have appeared to influence the work reported in this paper.

Acknowledgments

This work was supported in part by the National Natural Science Foundation of China, (No. 52277008,52130710), Natural Science Foundation of Hebei Province, China (No. E2023202050), and the Funds for Creative Research Groups of Hebei Province, China(No. E2024202298).

Data availability

The data that has been used is confidential.

References

[1] Q. Ding, J. Li, R. Zhang, et al., Effect of transverse magnetic field annealing on the magnetic properties and microstructure of FeSiBNbCuP nanocrystalline alloys, J. Magn. Magn. Mater. 560 (2022), https://doi.org/10.1016/j.jmmm.2022.169628.

[2] R. Zhang, A. He, L. Xie, et al., Correlation between dynamic magnetization process and dynamic domains of high saturation induction FeSiBNbCuMo nanocrystalline alloy with dual anisotropies, J. Alloy. Compd. 891 (2022), https://doi.org/10.1016/j.jallcom.2021.161956.

[3] J. Petzold, Applications of nanocrystalline soft magnetic materials for modern electronic devices, Scr. Mater. 48 (2003) 895–901, https://doi.org/10.1016/S1359-6462(02)00624-3.

[4] Z. Wan, Y. Li, H. Wang, et al., Optimization design of high-frequency matrix transformer for solid-state transformer, IEEE Trans. Power Electron. 39 (2025) 12384–12396, https://doi.org/10.1109/TPEL.2024.3424509.

[5] C. Jiang, X. Li, S.S. Ghosh, et al., Nanocrystalline powder cores for high-power high-frequency power electronics applications, IEEE Trans. Power Electron. 35 (2020) 10821–10830, https://doi.org/10.1109/TPEL.2020.2979069.

[6] Y. Liu, Y. Yi, W. Shao, et al., Microstructure and magnetic properties of soft magnetic powder cores of amorphous and nanocrystalline alloys, J. Magn. Magn. Mater. 330 (2012) 119–133, https://doi.org/10.1016/j.jmmm.2012.10.043.

[7] P. Fu, J. Shi, R. Shi, et al., Effect of low magnetic field heat treatment process on grain sizes and soft magnetic properties of Finemet cores, Mater. Today Commun. 36 (2023), https://doi.org/10.1016/j.mtcomm.2023.106685.

[8] P. Cai, A. He, N. Zhang, et al., Correlation between stress relaxation induced anisotropy, magnetic domain, and permeability of Co-doped FeCuSiBNbMn alloys, J. Magn. Magn. Mater. 588 (2023), https://doi.org/10.1016/j.jmmm.2023.171407.

[9] F. Sybille, et al., Magnetization loss and domain refinement in nanocrystalline tape wound cores, Acta Mater. 54 (2006) 3253–3259, https://doi.org/10.1016/j.actamat.2006.03.011.

[10] S. Chiroli, D. Faurie, M. Haboussi, et al., Magnetization dynamics of elastically strained nanostructures studied by coupled micromagnetic-mechanical simulations, Phys. Rev. B 108 (2023) 2, https://doi.org/10.1103/PhysRevB.108.024406.

[11] T. Sun, Q. Liu, M. Xie, Research progress on iron-based amorphous nanocrystalline alloy soft magnetic materials, Metallurgical Management 19 (2020) 25–26.

[12] Wu. Xiao Bin, L.Y. Yuqin, Machine learning research on nickel-based single crystal superalloy doping based on first-principles calculations, Shanghai Metal 42 (2020) 97–104.

[13] M.J. Donahue, R.D. McMichael, Micromagnetics on curved geometries using rectangular cells: error correction and analysis, IEEE Trans. Magn. 43 (2007) 2878–2880, https://doi.org/10.1109/TMAG.2007.892865.

[14] S.J. Lee, S. Sato, H. Yanagihara, et al., Numerical simulation of random magnetic anisotropy with solid magnetization grains, J. Magn. Magn. Mater. 323 (2011) 28–31, https://doi.org/10.1016/j.jmmm.2010.08.015.

[15] N.M. Saiden, T. Schrefl, H.A. Davies, et al., Micromagnetic finite element simulation of nanocrystalline α-Fe/Nd2Fe14B/Fe3B magnets, J. Magn. Magn. Mater. 365 (2014) 45–50, https://doi.org/10.1016/j.jmmm.2014.02.073.

[16] J. Zhang, Y. Wang, J. Xue, et al., Micromagnetic simulation of shape anisotropy effect of magnetic nanosystems, Magnetic Materials and Devices 44 (2013) 13–16.

[17] L. Dai, L. Zou, K. Guo, et al., Analysis of the influence of nanocrystalline alloy grain size and volume fraction on high-frequency magnetic loss characteristics, Electric Power Technology Journal 38 (2023) 4853–4863.

[18] L. Zhang, Y. Wang, L. Zou, et al., Effect of grain size on magnetic loss of nanocrystalline alloy under high-frequency non-sinusoidal excitation, IEEE Trans. Magn. 59 (2023) 1–11, https://doi.org/10.1109/TMAG.2023.3277075.

[19] Z. Han, L. Zou, J. Wu, et al., Micromagnetic analysis of the influence of external and internal factors on the kHz-level saturation magnetization process of nanocrystalline alloys, Journal of Electrical Technology 34 (2019) 1589–1598.

[20] R. Skomski, J.M.D. Coey, Giant energy product in nanostructured two-phase magnets, Phys. Rev. B 48 (1993) 15812, https://doi.org/10.1103/PhysRevB.48.15812.

[21] G. Herzer, Grain structure and magnetism of nanocrystalline ferromagnets, IEEE Trans. Magn. 25 (1989) 3327–3329, https://doi.org/10.1103/PhysRevB.48.15812.

[22] G. Herzer, Modern soft magnets: Amorphous and nanocrystalline materials, Acta Mater. 61 (2013) 718–734, https://doi.org/10.1016/j.actamat.2012.10.040.

[23] G. Herzer, Magnetization process in nanocrystalline ferromagnets, Mater. Sci. Eng. A 133 (1991) 1–5, https://doi.org/10.1016/0921-5093(91)90003-6.

[24] K.S. Sivaranjani, G.A. Jacob, R.J. Joseyphus, comprehensive law-of-approach-to-saturation for the determination of magnetic anisotropy in soft magnetic Materials, Physica Status Solidi (b) 259 (2022) 2200050, https://doi.org/10.1002/pssb.202200050.

[25] S. Chikazumi, Physics of Magnetism, Wiley, New York, 1964, p. 274.

[26] K. Suzuki, J.M. Cadogan, Random magnetocrystalline anisotropy in two-phase nanocrystalline systems, Phys. Rev. B 58 (1998) 2730, https://doi.org/10.1103/PhysRevB.58.2730.

[27] J.E. Miltat, M.J. Donahue, Numerical micromagnetics: Finite difference methods, Handbook of Magnetism and Advanced Magnetic Materials 2 (2007) 742–764.

[28] A.S. Bolyachkin, S.V. Komogortsev, Power-law behavior of coercivity in nanocrystalline magnetic alloys with grain-size distribution, Scr. Mater. 152 (2018) 55–58, https://doi.org/10.1016/j.scriptamat.2018.04.008.